Inorganic Chemistry

Article

pubs.acs.org/IC

# Four Coordination Polymers Based on Identical Eight-Connected Heptanuclear Clusters: Spin Canting, Spin Glass, Antiferromagnetism, and Gas Adsorption

Jia Li,[†] Bao Li,[‡] Peng Huang,[†] Hai-Yan Shi,*[,†] Rong-Bin Huang,[†] Lan-Sun Zheng,[†] and Jun Tao*[,†]

[†]State Key Laboratory of Physical Chemistry of Solid Surfaces and College of Chemistry and Chemical Engineering, Xiamen University, Xiamen 361005, People's Republic of China.

[‡]School of Chemistry and Chemical Engineering, Huazhong University of Science and Technology, Wuhan 430074, People's Republic of China

Supporting Information

**ABSTRACT:** Four 3D coordination polymers, $[Co_7(OH)_4(H_2O)_2(ina)_4(ip)_3]\cdot 10H_2O$ (**1**·$10H_2O$, ina = isonicotinate, ip = isophthalate), $[Ni_7(OH)_4(H_2O)_2(ina)_4(ip)_3]\cdot 10H_2O$ (**2**·$10H_2O$), $[Co_7(OH)_4(H_2O)_2(ina)_4(pip)_3]\cdot 5H_2O$ (**3**·$5H_2O$, pip = 5-phenyl-isophthalate), and $[Ni_7(OH)_4(H_2O)_2(ina)_4(pip)_3]\cdot 5H_2O$ (**4**·$5H_2O$), respectively, were hydrothermally synthesized. They crystallized in the orthorhombic space group *Pba*2 for **1**·$10H_2O$ and **2**·$10H_2O$ and monoclinic space group *P*2/*n* for **3**·$5H_2O$ and **4**·$5H_2O$, respectively, and were constructed with the identical 8-connected heptanuclear $\{M_7(OH)_4\}$ (M = $Co^{II}$ or $Ni^{II}$) clusters, possessing uninodal hexagonal primitive net with the point symbol $\{3^6\cdot4^{18}\cdot5^3\cdot6\}$. The four coordination polymers showed dominant antiferromangetic properties, in which **1**·$10H_2O$ shows spin-canted behavior and **2**·$10H_2O$ exhibits the coexistence of spin canting and spin glass. Meanwhile, the activated polymers **1** and **2** possessed permanent porosity, displaying relatively large $H_2$ uptake capacity (77 K, 1 atm) of 114 and 133 $cm^3\ g^{-1}$, and $CO_2$ uptake capacity (273 K, 1 atm) of 65.8 and 73.3 $cm^3\ g^{-1}$, for **1** and **2**, respectively.

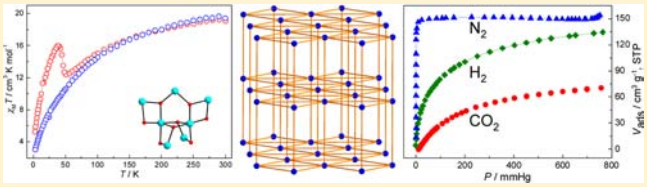


## INTRODUCTION

Coordination polymers (CPs) constructed with metal ions and various organic ligands have attracted considerable interest owing to their promising applications in gas storage, catalysis, and magnetic materials.[1−3] Recently, much effort has been devoted to the design of high-connectivity CPs based on polynuclear metal clusters, which can not only avoid structural interpenetration and increase porosity of frameworks, but also contribute novel topological structures and functionalities.[4] Especially, magnetic CPs constructed with high-nuclearity clusters are good examples to better understand some magnetic phenomena (e.g., ferromagnetism, antiferromagnetism, spin canting, spin glass, metamagnetic, and spin-flop transition),[5] because the nature of magnetic couplings in metal cluster-based CPs depends on various factors, including the coordination modes of carboxylate groups, anisotropy of metal ions, the orientation of neighboring coordination geometries, etc.[6] On the other hand, multifunctional CPs exhibiting at least two different physical properties are very important in chemistry and materials science. For example, some CPs show the coexistence of magnetic properties and nonlinear optical, ferroelectric, or dielectric properties,[7,8] and some CPs show magnetic properties and porous nature.[9]

The construction of CPs that simultaneously possess magnetic properties and porosity is one of the major challenges in multifunctional materials. To our knowledge, such CPs with high-connected nodes are relatively rare;[10,11] among them, metal clusters usually act as the high-connected nodes, and multidentate carboxylate ligands are often employed to connect them. In these cases, the peripheral metal ions of metal clusters are usually coordinated by terminal neutral solvent molecules, which could be replaced by neutral pyridyl ligands to increase the connectivity of CPs.[12] Bearing this in mind, we have tried to synthesize high-connectivity metal cluster-based CPs by adopting carboxylate and pyridyl-carboxylate ligands. In this Article, we report the synthesis and characterization of four 8-connected CPs that are constructed with heptanuclear metal clusters and mixed isophthalate (or 5-phenyl-isophthalate) and isonicotinate ligands (Scheme 1), i.e.,

**Scheme 1. Molecular Structures of $H_2$ip, $H_2$pip, and Hina**

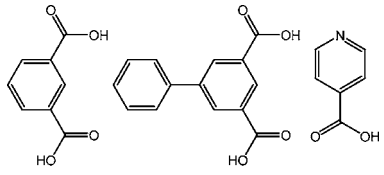


**Received:** July 23, 2013
**Published:** September 25, 2013

   dx.doi.org/10.1021/ic401912k | *Inorg. Chem.* 2013, 52, 11573−11579

Table 1. Crystal Data and Structure Refinements for the Four Complexes

| | 1·10$H_2O$ | 2·10$H_2O$ | 3·5$H_2O$ | 4·5$H_2O$ |
|---|---|---|---|---|
| formula | $C_{48}H_{56}N_4Co_7O_{36}$ | $C_{48}H_{56}N_4Ni_7O_{36}$ | $C_{66}H_{61}N_4Co_7O_{31}$ | $C_{66}H_{61}N_4Ni_7O_{31}$ |
| $M_r$/g mol$^{-1}$ | 1677.50 | 1675.82 | 1818.73 | 1817.05 |
| cryst syst | orthorhombic | orthorhombic | monoclinic | monoclinic |
| space group | *Pba*2 | *Pba*2 | *P*2/*n* | *P*2/*n* |
| *a*/Å | 13.848(6) | 13.722(2) | 13.7453(8) | 13.6192(8) |
| *b*/Å | 19.978(9) | 19.730(3) | 13.1307(5) | 12.9919(6) |
| *c*/Å | 13.111(6) | 12.988(2) | 20.5544(11) | 20.3610(10) |
| $\alpha$/deg | 90.00 | 90.00 | 90.00 | 90.00 |
| $\beta$/deg | 90.00 | 90.00 | 103.322(6) | 103.612(5) |
| $\gamma$/deg | 90.00 | 90.00 | 90.00 | 90.00 |
| *V*/Å$^3$ | 3627(3) | 3516.3(10) | 3609.9(3) | 3501.5(3) |
| *Z* | 2 | 2 | 2 | 2 |
| $D_c$/g cm$^{-3}$ | 1.367 | 1.409 | 1.610 | 1.628 |
| $\mu$/mm$^{-1}$ | 1.63 | 1.905 | 1.653 | 1.925 |
| reflns collected | 20 823 | 19 607 | 17 354 | 14 722 |
| GOF | 0.859 | 1.028 | 1.090 | 1.040 |
| $R_{int}$ | 0.0545 | 0.0426 | 0.1112 | 0.0524 |
| R1 ($I > 2\sigma(I)$)[a] | 0.0441 | 0.0407 | 0.0896 | 0.0445 |
| wR2 (all data) | 0.0770 | 0.1050 | 0.1996 | 0.1203 |

[a] $R1 = ||F_o| - |F_c||/|F_o|$; $wR2 = \{[w(F_o^2 - F_c^2)^2]/[w(F_o^2)^2]\}^{1/2}$; $w = 1/[\sigma_2(F_o^2) + (ap)^2 + bp]$, where $p = [\max(F_o^2, 0) + 2F_c^2]/3$; and $Rw = [w(|F_o| - |F_c|)^2/w|F_o|^2]^{1/2}$, where $w = 1/\sigma^2(|F_o|)$.

$[M_7(OH)_4(H_2O)_2(L1)_4(L2)_3]\cdot xH_2O$ (M = $Co^{II}$, L1 = ina, L2 = ip, *x* = 10 for 1·10$H_2O$; M = $Ni^{II}$, L1 = ina, L2 = ip, *x* = 10 for 2·10$H_2O$; M = $Co^{II}$, L1 = ina, L2 = pip, *x* = 5 for 3·5$H_2O$; M = $Ni^{II}$, L1 = ina, L2 = pip, *x* = 5 for 4·5$H_2O$). The absence or presence of phenyl group on isophthalate ligand (i.e., ip vs pip) plays an important role in affecting the magnetic and adsorptive properties of the four CPs.

## EXPERIMENTAL SECTION

**Materials and Physical Measurements.** All starting materials were purchased commercially and were used without further purification. Elemental analyses for C, H, and N were performed on Perkin-Elmer 240Q elemental analyzer. The IR spectra (KBr pellets) were recorded in the range 400−4000 cm$^{-1}$ on a Nicolet 5DX spectrometer. Thermogravimetric analysis (TGA) was performed at a rate of 10 °C/min under nitrogen on NETZSCH TG 209 system. Powder X-ray diffraction (PXRD) studies were performed on Panalytical X-Pert PRO diffractometer with Cu K$\alpha$ radiation ($\lambda$ = 0.154 18 nm, 40.0 kV, 30.0 mA). Gas sorption isotherms were performed on Micromeritics ASAP 2020 system. Magnetic susceptibility measurements were carried out on a Quantum Design MPMS XL7 SQUID magnetometer in the 2−300 K temperature range under magnetic field of 1000 Oe. Magnetic data were calibrated with the sample holder, and diamagnetic corrections were estimated from Pascal's constants.

**Synthesis.** The synthesis for $[Co_7(OH)_4(H_2O)_2(ina)_4(ip)_3]\cdot 10H_2O$ (1·10$H_2O$) follows: Solid $Co(NO_3)_2\cdot 6H_2O$ (0.208 g, 0.7 mmol) was added without stirring to an EtOH/$H_2O$ (10 mL, v/v = 3:7) solution containing isonicotinic acid (0.062 g, 0.5 mmol), isophthalic acid (0.083 g, 0.5 mmol), and NaOH (0.060 g, 1.5 mmol). The mixture was sealed in a 23 mL Teflon-lined stainless steel vessel and heated to 160 °C within 500 min, maintained at this temperature for 3600 min, and then cooled to 30 °C within 2880 min. Red block crystals of 1·10$H_2O$ were obtained by filtration. Yield: ∼75% based on $Co(NO_3)_2\cdot 6H_2O$. Anal. Calcd (%) for $C_{48}H_{56}N_4Co_7O_{36}$: C 34.36, H 3.36, N 3.34. Found: C 34.52, H 3.37, N 3.32. IR (KBr, cm$^{-1}$): 3425, 1616, 1554, 1478, 1339, 754, 709, 689, 441.

The synthesis for $[Ni_7(OH)_4(H_2O)_2(ina)_4(ip)_3]\cdot 10H_2O$ (2·10$H_2O$) follows: Solid $Ni(NO_3)_2\cdot 6H_2O$ (0.206 g, 0.7 mmol) was added without stirring to an aqueous solution (10 mL) of isonicotinic acid (0.025 g, 0.2 mmol), isophthalic acid (0.0664 g, 0.4 mmol), and NaOH (0.045 g, 1.1 mmol). The mixture was sealed in a 23 mL Teflon-lined stainless steel vessel and heated to 185 °C within 500 min, maintained at this temperature for 3600 min, and then cooled to 30 °C within 2880 min. Blue-green block crystals of 2·10$H_2O$ were obtained by filtration. Yield: ∼81% based on Hina. Anal. Calcd (%) for $C_{48}H_{56}N_4Ni_7O_{36}$: C 34.40, H 3.37, N 3.34. Found: C 34.18, H 3.41, N 3.32. IR (KBr, cm$^{-1}$): 3450, 1611, 1557, 1478, 1416, 1390, 754.16, 714, 693, 446.

The synthesis for $[Co_7(OH)_4(H_2O)_2(ina)_4(pip)_3]\cdot 5H_2O$ (3·5$H_2O$) follows: Isonicotinic acid (0.025 g, 0.2 mmol), 5-phenyl-isophthalic acid (0.0968 g, 0.4 mmol), and NaOH (0.028 g, 0.7 mmol) were added to 5 mL of water, the mixture was stirred for 30 min and then transferred to a 23 mL Teflon-lined stainless steel vessel. EtOH (5 mL) and then solid $Co(OAc)_2\cdot 4H_2O$ (0.1743 g, 0.7 mmol) were added to the solution without stirring. The vessel was sealed and heated to 160 °C within 500 min, maintained at this temperature for 3600 min, and then cooled to 30 °C within 2880 min. Red block crystals of 3·5$H_2O$ were separated by filtration. Yield: ∼ 70% based on Hina. Anal. Calcd (%) for $C_{66}H_{61}N_4Co_7O_{31}$: C 43.58, H 3.38, N 3.08. Found: C 43.62, H 3.23, N 3.00. IR (KBr, cm$^{-1}$): 3408, 2975, 1617, 1565, 1499, 1418, 1396, 1089, 1048, 879, 778, 757, 714, 628, 446.

The synthesis for $[Ni_7(OH)_4(H_2O)_2(ina)_4(pip)_3]\cdot 5H_2O$ (4·5$H_2O$) follows: Isonicotinic acid (0.025 g, 0.2 mmol), 5-phenyl-isophthalic acid (0.0968 g, 0.4 mmol), and NaOH (0.040 g, 1.0 mmol) were added to 10 mL of water, and the mixture was stirred for 30 min and then transferred to a 23 mL Teflon-lined stainless steel vessel. Solid $Ni(OAc)_2\cdot 4H_2O$ (0.1742 g, 0.7 mmol) was then added without stirring to the solution. The vessel was sealed and heated to 160 °C within 500 min, maintained at this temperature for 3600 min, and then cooled to 30 °C within 2880 min. Green block crystals of 4·5$H_2O$ were separated by filtration. Yield: ∼90% based on Hina. Anal. Calcd (%) for $C_{66}H_{61}N_4Ni_7O_{31}$: C 43.62, H 3.38, N 3.08. Found: C 43.56, H 3.27, N 3.04. IR (KBr, cm$^{-1}$): 3435, 1616, 1556, 1499, 1418, 1394, 1213, 1073, 1057, 869, 779, 761, 719, 628, 434.

**Crystallographic Data Collection and Structure Determination.** Diffraction data were collected on Rigaku Image Plate and Oxford Gemini S Ultra diffractometers equipped with Mo K$\alpha$ ($\lambda$ = 0.710 73 Å). The crystal structures were solved and refined using the SHELXTL program suite.[13] Direct methods yielded all nonhydrogen atoms, which were refined anisotropically, while all hydrogen atoms were calculated geometrically and were riding on their respective atoms. In all compounds, disordered lattice water molecules were


dx.doi.org/10.1021/ic401912k | Inorg. Chem. 2013, 52, 11573−11579

Table 2. Selected Bond Lengths (Å) for the Four Compounds[a]

| | | | | | | | |
|---|---|---|---|---|---|---|---|
| **1**·10H$_2$O | | | | **2**·10H$_2$O | | | |
| Co(1)−O(11) | 2.067(3) | Co(3)−O(6) | 2.090(3) | Ni(1)−O(9) | 2.038(3) | Ni(3)−O(6) | 2.044(3) |
| Co(1)−O(9) | 2.107(3) | Co(3)−O(12a) | 2.113(3) | Ni(1)−O(11) | 2.040(3) | Ni(3)−O(12a) | 2.058(3) |
| Co(1)-O(4b) | 2.109(3) | Co(3)−O(1) | 2.106(3) | Ni(1)-O(4b) | 2.086(3) | Ni(3)−O(1) | 2.065(3) |
| Co(2)−O(11) | 2.042(3) | Co(3)−O(7) | 2.132(3) | Ni(2)-O(3c) | 2.015(3) | Ni(3)−O(7) | 2.102(3) |
| Co(2)−O(3b) | 2.051(3) | Co(4)−O(12) | 2.027(3) | Ni(2)−O(11) | 2.020(3) | Ni(4)−O(1W) | 1.981(5) |
| Co(2)−O(10a) | 2.134(3) | Co(4)−O(8a) | 2.074(3) | Ni(2)−O(10a) | 2.090(3) | Ni(4)−O(12) | 2.017(3) |
| Co(2)−N(2d) | 2.135(3) | Co(4)−O(1W) | 2.089(3) | Ni(2)−N(2d) | 2.108(3) | Ni(4)−O(8a) | 2.035(3) |
| Co(2)−O(5) | 2.163(3) | Co(4)−O(2) | 2.089(3) | Ni(2)−O(5) | 2.109(3) | Ni(4)−N(1e) | 2.059(4) |
| Co(2)−O(7) | 2.219(3) | Co(4)−N(1e) | 2.111(4) | Ni(2)−O(7) | 2.183(3) | Ni(4)−O(2) | 2.068(3) |
| Co(3)−O(12) | 2.041(3) | Co(4)−O(1a) | 2.211(3) | Ni(3)−O(12) | 2.007(3) | Ni(4)−O(1a) | 2.143(3) |
| Co(3)−O(11) | 2.066(3) | | | Ni(3)−O(11) | 2.021(3) | | |
| **3**·5H$_2$O | | | | **4**·5H$_2$O | | | |
| Co(1)−O(11) | 2.060(6) | Co(3)−O(11) | 2.073(6) | Ni(1)−O(9) | 2.005(4) | Ni(3)-O(12a) | 2.030(3) |
| Co(1)−O(9b) | 2.062(10) | Co(3)−O(12) | 2.092(8) | Ni(1)−O(11) | 2.033(3) | Ni(3)−O(12) | 2.047(3) |
| Co(1)−O(4d) | 2.088(6) | Co(3)−O(1) | 2.100(6) | Ni(1)−O(4b) | 2.061(4) | Ni(3)−O(1) | 2.064(3) |
| Co(2)−O(11) | 2.039(5) | Co(3)−O(7) | 2.135(6) | Ni(2)−O(11) | 2.010(3) | Ni(3)−O(7d) | 2.100(3) |
| Co(2)−O(3e) | 2.039(6) | Co(4)−O(12) | 2.025(6) | Ni(2)−O(3c) | 2.013(3) | Ni(4)−O(12) | 2.014(3) |
| Co(2)−O(10a) | 2.120(8) | Co(4)−O(2c) | 2.078(6) | Ni(2)−O(10) | 2.084(3) | Ni(4)−N(1e) | 2.057(4) |
| Co(2)−N(2f) | 2.139(8) | Co(4)−N(1) | 2.105(11) | Ni(2)−N(2) | 2.090(4) | Ni(4)−O(2a) | 2.059(3) |
| Co(2)−O(5) | 2.153(9) | Co(4)−O(8) | 2.107(6) | Ni(2)−O(5) | 2.102(3) | Ni(4)−O(8d) | 2.065(3) |
| Co(2)−O(7) | 2.228(6) | Co(4)−O(1W) | 2.136(7) | Ni(2)−O(7d) | 2.182(3) | Ni(4)−O(1W) | 2.091(3) |
| Co(3)−O(6) | 2.037(9) | Co(4)−O(1) | 2.198(8) | Ni(3)−O(6) | 2.020(3) | Ni(4)−O(1) | 2.121(3) |
| Co(3)−O(12c) | 2.055(6) | | | Ni(3)−O(11) | 2.023(3) | | |

[a]Symmetry codes: (a) $-x+1, -y+2, z$; (b) $x, y, z-1$; (c) $-x+1, -y+2, z-1$; (d) $-x+{}^3/_2, y+{}^1/_2, z$; (e) $-x+{}^3/_2, y-{}^1/_2, z$; (f) $x-{}^1/_2, -y+{}^3/_2, z$; (g) $x-{}^1/_2, -y+{}^5/_2, z$ for **1**·10H$_2$O. (a) $-x+1, -y, z$; (b) $-x+1, -y, z-1$; (c) $x, y, z-1$; (d) $-x+{}^3/_2, y-{}^1/_2, z$; (e) $-x+{}^3/_2, y+{}^1/_2, z$; (f) $x-{}^1/_2, -y+{}^1/_2, z$; (g) $x-{}^1/_2, -y-{}^1/_2, z$ for **2**·10H$_2$O. (a) $-x, -y+1, -z+1$; (b) $x+{}^1/_2, -y+1, z+{}^1/_2$; (c) $-x+{}^1/_2, y, -z+{}^3/_2$; (d) $-x+{}^1/_2, y-1, -z+{}^3/_2$; (e) $x, y-1, z$; (f) $-x+1, -y+1, -z+1$; (g) $x-1/2, -y+1, z+{}^1/_2$ for **3**·5H$_2$O. (a) $-x+{}^1/_2, y, -z+{}^1/_2$; (b) $-x+{}^1/_2, y-1, -z+{}^1/_2$; (c) $x, y-1, z$; (d) $-x, -y+1, -z+1$; (e) $-x+1, -y+1, -z+1$; (f) $x+{}^1/_2, -y+1, z-{}^1/_2$; (g) $x-{}^1/_2, -y+1, z-{}^1/_2$ for **4**·5H$_2$O.

removed during structural refinement via application of the Squeeze function in PLATON.[14] Crystallographic data and structural refinement details are presented in Table 1. Selected bonds distances are summarized in Table 2.

## RESULTS AND DISCUSSION

**Crystal Structures.** Single-crystal X-ray diffraction studies reveal that **1**·10H$_2$O and **2**·10H$_2$O crystallize in the orthorhombic space group *Pba*2 while **3**·5H$_2$O and **4**·5H$_2$O crystallize in the monoclinic space group *P*2/*n*. Complexes **1**−**4** are 3D noninterpenetrated structures with isostructural heptanuclear metal clusters connected by isonicotinate and isophthalate/5-phenyl-isophthalate ligands. As shown in Figure 1 and Figures S1−S4 (Supporting Information), the heptanuclear cluster has a $C_2$ symmetric axis, and each metal ion locates in a distorted octahedral geometry. The M1 atom is coordinated by four oxygen atoms from different carboxylate groups and two $\mu_3$-OH$^-$ groups; the M2 atom is coordinated by four oxygen atoms from four carboxylate groups, one nitrogen atom of ina and one $\mu_3$-OH$^-$ group; the M3 atom is coordinated by three oxygen atoms from different carboxylate groups and three $\mu_3$-OH$^-$ groups; the M4 atom is coordinated by three oxygen atoms from different carboxylate groups, one nitrogen atom of ina, one $\mu_3$-OH$^-$ group, and one terminal water molecule. The M−O distances are 2.031(4)−2.228(15), 2.010(3)−2.191(3), 2.005(4)−2.230(6), and 2.010(3)−2.182(3) Å for **1**−**4**, respectively. The M−N distances range from 2.124(6) to 2.135(5), 2.106(4) to 2.161(4), 2.113(10) to 2.142(6), and 2.057(4) to 2.089(4) Å for **1**−**4**, respectively.

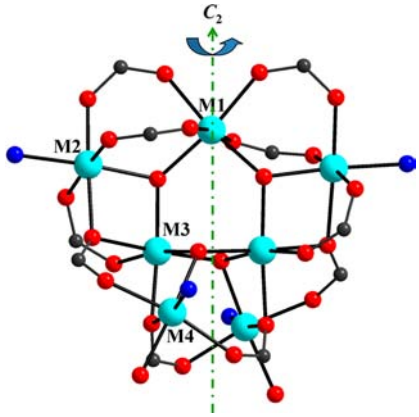


**Figure 1.** Perspective view of the heptanuclear metal cluster in **1**−**4**: cyan, Co$^{II}$ or Ni$^{II}$; red, O; blue, N; black, C.

Each heptanuclear cluster is bound to eight isonicotinate and six isophthalate or 5-phenyl-isophthalate ligands. Therefore, it is connected to eight neighboring ones through these ligands to yield a 3D framework (Figure 2). By taking the heptanuclear cluster as 8-connecting node, the topological structure of the four compounds can be assigned to the uninodal 8-connected hexagonal primitive net (Figure 2c) with point symbol $\{3^6{\cdot}4^{18}{\cdot}5^3{\cdot}6\}$, as calculated using TOPOS software.[15]

In the frameworks **1** and **2**, the guest water molecules reside in the 2D channels that are generated by interconnection of irregular cavities (Figure 3). The void spaces are corresponding to the trigonal windows along the *c*-axis direction, being 15.4% and 15.9% of the unit cell volumes for **1** and **2**, respectively. It


dx.doi.org/10.1021/ic401912k | Inorg. Chem. 2013, 52, 11573−11579

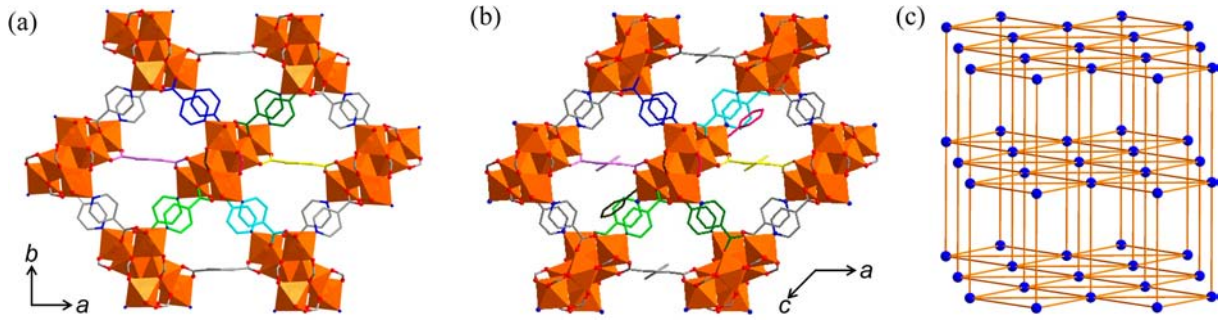


**Figure 2.** Three-dimensional structures of **1** (or **2**) viewed along the *c*-axis (a), **3** (or **4**) viewed along the *b*-axis (b), and the topological structure of **1**–**4** (c).

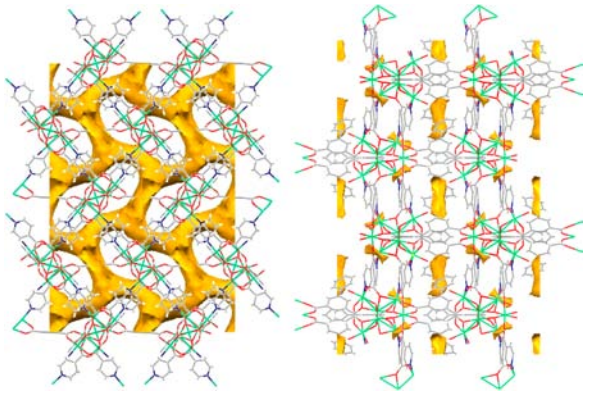

**Figure 3.** Accessible surfaces of **1** (or **2**, left) and **3** (or **4**, right).

should be noted that the removal of all coordinated water molecules would open new spaces, which then connect the former cavities and expand the void spaces to 35.7% and 36.7% for **1** and **2**, respectively. However, the accessible void volumes decrease to 15.8% and 15.2% of the unit cell volumes (after removal of all coordinated water molecules) for **3** and **4**, respectively, due to the existence of phenyl group on ip ligand.

**Thermal Stability.** The four compounds exhibit similar thermal stability under $N_2$. The TGA studies (Figure 4a) reveal that the first-step weight losses between 30 and 200 °C are 10.74%, 10.75%, and 4.95% for **1**·10$H_2O$, **2**·10$H_2O$, and **3**·5$H_2O$, respectively, which can be attributed to the release of guest water molecules (theoretically 11.37%, 11.44%, and 5.15% for **1**·10$H_2O$, **2**·10$H_2O$, and **3**·5$H_2O$, respectively). The second-step weight losses above 300 °C are 2.15%, 2.15%, and 1.98% for **1**, **2**, **3**, respectively, which correspond to the losses of coordinate water molecules (theoretically 2.20%, 2.22%, and 2.47% for **1**, **2**, and **3**, respectively). However, the weight losses of the guest and coordinate water molecules for **4**·5$H_2O$ are not well resolved. Instead, a total weight loss of 6.94% below 350 °C has been found, in agreement with the theoretical one (7.08%) for in total seven water molecules. To further examine the thermal stability of frameworks, samples **1**·10$H_2O$ and **2**·10$H_2O$ were heated at various temperatures under $N_2$ gas flow, and then powder X-ray diffraction studies were performed. The PXRD patterns reveal that the frameworks **1** and **2** remain intact until 300 °C (Figure 4b,c). On the other hand, the two cobalt complexes (**1**·10$H_2O$ and **3**·5$H_2O$) change from red to black and the two nickel complexes (**2**·10$H_2O$ and **4**·5$H_2O$) from green to pale yellow green, respectively, after being heated at 220 °C for 10 h in vacuum. Interestingly, by immersing the anhydrous samples in aqueous solution for several hours, the samples completely recover the original colors. This dynamic phenomenon suggests a reversible desorption–adsorption of guest and coordinate water molecules.

**Magnetic Properties.** The magnetic susceptibilities of microcrystalline samples of **1**·10$H_2O$, **2**·10$H_2O$, **3**·5$H_2O$, and **4**·5$H_2O$ were measured in the temperature range 2–300 K under applied field of 1000 Oe. The room temperature $\chi_M T$ value (per $Co^{II}_7$ unit) for **1**·10$H_2O$ is 19.08 $cm^3$ K $mol^{-1}$ (Figure 5a), which is much higher than the spin-only value of 13.13 $cm^3$ K $mol^{-1}$ expected for seven isolated $Co^{II}$ ions ($S = {}^3/_2$, $g = 2.0$) indicating the presence of orbital contribution of high-spin $Co^{II}$ ion in octahedral field. The $\chi_M T$ value gradually decreases upon cooling and attains a minimum of 12.45 $cm^3$ K $mol^{-1}$ at 50 K, and then shows a rapid increase to a maximum of 15.98 $cm^3$ K $mol^{-1}$ at 38 K, followed by gradual decrease to 5.29 $cm^3$ K $mol^{-1}$ at 2 K. This type of magnetic behavior indicates a canted antiferromagnetism,[16] and the final decrease of the $\chi_M T$ value suggests antiferromagnetic interactions among the neighboring $\{Co^{II}_7\}$ chains or layers and/or magnetic anisotropy of $Co^{II}$ ions.[17] A fit of the $\chi_M{}^{-1}$ data above 50 K to the Curie–Weiss

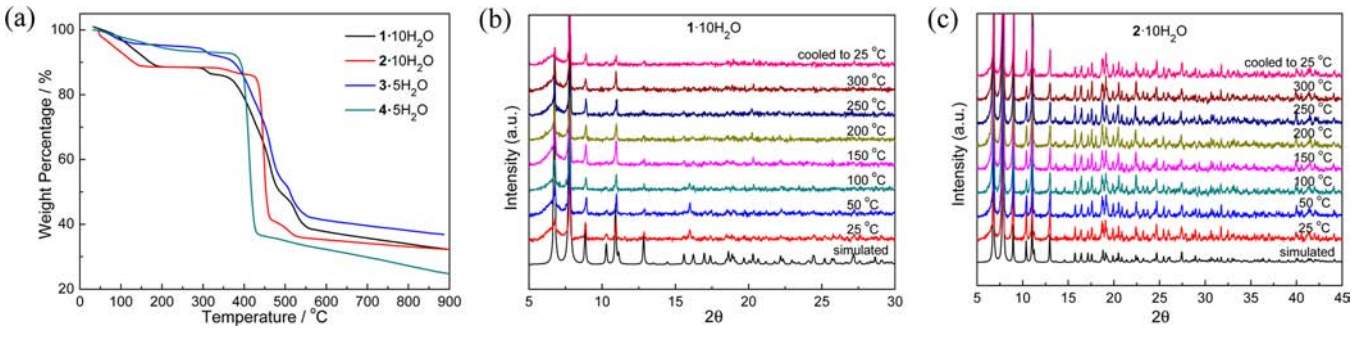


**Figure 4.** TGA pattern of the four complexes (a), and the variable temperature PXRD patterns of **1**·10$H_2O$ (b), and **2**·10$H_2O$ (c).


dx.doi.org/10.1021/ic401912k | *Inorg. Chem.* 2013, 52, 11573–11579

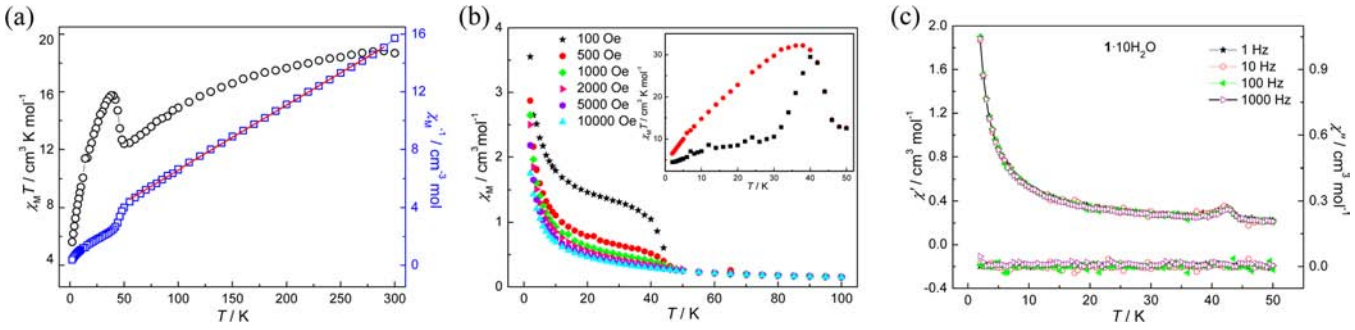


**Figure 5.** $\chi_M T$ vs $T$ plot (per $Co^{II}_7$) of **1**·10$H_2O$ under applied field of 1000 Oe (a), the field-dependent magnetic susceptibilities of **1**·10$H_2O$ below 100 K (b, inset: ZFC and FC magnetization at 50 Oe warming from 2 K), and the in-phase and out-of-phase ac susceptibility for **1**·10$H_2O$ in zero dc and 3 Oe ac applied field (c).

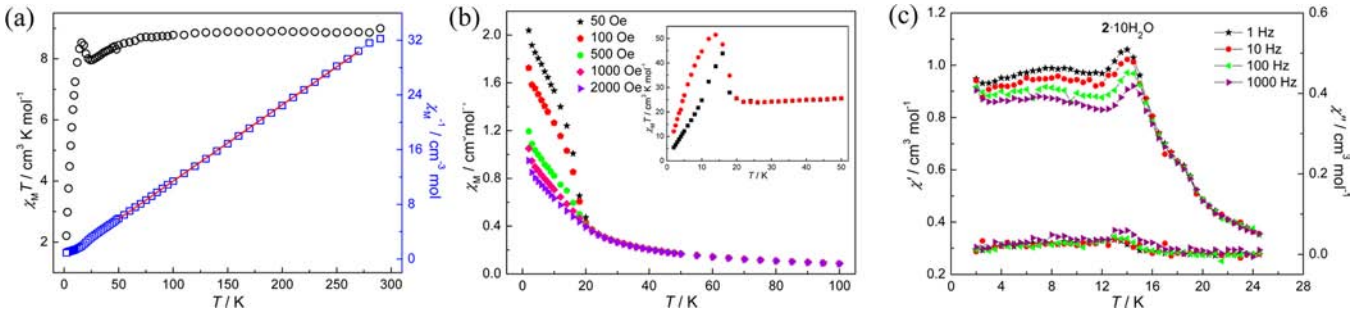


**Figure 6.** $\chi_M T$ vs $T$ plot (per $Ni^{II}_7$) of **2**·10$H_2O$ under applied field of 1000 Oe (a), the field-dependent magnetic susceptibilities of **2**·10$H_2O$ below 100 K (b, inset: ZFC and FC magnetization at 50 Oe warming from 2 K), and the in-phase and out-of-phase ac susceptibility for **2**·10$H_2O$ in zero dc and 3 Oe ac applied field (c).

law gives a Curie constant $C$ = 22.4 $cm^3$ K $mol^{-1}$ and a Weiss temperature $\theta$ = −47.39 K. The negative $\theta$ value may indicate the presence of overall antiferromagnetic interactions within the $Co^{II}_7$ cluster as well as the spin−orbit coupling effects of octahedral $Co^{II}$ ions with a $^4T_{1g}$ ground term.

It is noticeable that the magnetic susceptibility shows strong field dependence below 43 K (Figure 5b). By applying different magnetic fields, the magnetic susceptibility increases with decreasing magnetic field because of small spontaneous magnetization of canted antiferromagnetism. In order to characterize the low-temperature behaviors, the field-cooled (FC) and zero-field-cooled (ZFC) magnetizations were measured at 50 Oe upon warming from 2 K (Figure 5b, inset). The ZFC and FC plots completely diverge below 42 K, suggesting the onset of long-range antiferromagnetic ordering. The critical temperature ($T_c$) ascertained in the ZFC-FC plots is in agreement with that observed in the temperature-dependent alternating current (ac) susceptibilities (Figure 5c). The maximum of in-phase signal ($\chi'$) is 42 K, confirming the occurrence of one magnetic phase transition, while the negligible out-of-phase signal ($\chi''$) suggests a small canting angle.[18]

The isothermal magnetization at 2 K is far from saturation, reaching a value of 6.20 $N\beta$ at 7 T (Figure S9 in the Supporting Information). The complex exhibits a hysteresis loop at 2 K with a coercive field of ∼53 Oe and remanent magnetization of 0.011 $N\beta$ (Figure S13 in the Supporting Information). The canting angle can then be estimated to be about 0.04° based on the equation[19] $\alpha = \tan^{-1}(M_r/M_s)$ ($M_s$ = 15.16 $N\beta$, $S' = {}^1/_2$ and $g'$ = 4.33 for octahedral $Co^{II}$ at 2 K).

The magnetic behavior of **2**·10$H_2O$ highly resembles that of **1**·10$H_2O$ (Figure 6a). The $\chi_M T$ value of **2**·10$H_2O$ is 8.99 $cm^3$ K $mol^{-1}$ at room temperature, which is slightly higher than the spin-only value of 7.00 $cm^3$ K $mol^{-1}$ expected for seven isolated $Ni^{II}$ ions ($S$ = 1, $g$ = 2.0). Below 100 K, the $\chi_M T$ value gradually decreases upon cooling and reaches a minimum of 7.96 $cm^3$ K $mol^{-1}$ at 24 K, and then shows a rapid increase to a maximum of 8.53 $cm^3$ K $mol^{-1}$ at 16 K, followed by abrupt decrease to 2.21 $cm^3$ K $mol^{-1}$ at 2 K. This type of magnetic behavior is characteristic of a canted antiferromagnetism, and the final decrease of the $\chi_M T$ value suggests antiferromagnetic interactions among the neighboring $\{Ni^{II}_7\}$ chains or layers. The $\chi_M{}^{-1}$ data above 25 K were fitted with the Curie−Weiss law, giving a Curie constant $C$ = 8.96 $cm^3$ K $mol^{-1}$ and a Weiss temperature $\theta$ = −1.96 K. The negative $\theta$ value clearly indicates the presence of overall antiferromagnetic interactions within the $Ni^{II}_7$ cluster.

Meanwhile, the magnetic susceptibility of **2**·10$H_2O$ at low temperature (below 20 K) shows the same field-induced response as that of **1**·10$H_2O$ (Figure 6b), confirming the occurrence of spin canting. The ZFC and FC susceptibilities diverge at 16 K, suggesting the onset of long-range antiferromagnetic ordering. However, these results are not fully in line with that observed in the temperature-dependent ac susceptibilities. As depicted in Figure 6c, a slight frequency-dependent behavior is observed in the ac susceptibility. The frequency shift parameter can be estimated by the equation $\Phi = \Delta T_p/[T_p \Delta(\log\omega)]$, where $T_p$ is the peak temperature and $\omega$ is the frequency. The value of $\Phi$ is 0.012, in good accordance with a spin-glass behavior.[20] All these features suggest that **2**·10$H_2O$ shows the coexistence of spin-canted antiferromagnetism and spin glass.

The linear increase in the field-dependent magnetization at 2 K is associated with antiferromagnetic interactions; the


dx.doi.org/10.1021/ic401912k | Inorg. Chem. 2013, 52, 11573−11579

magnetization exhibits a value of 8.09 $N\beta$ at 7 T (Figure S10 in the Supporting Information) that is far from the theoretical saturation magnetization of $Ni^{II}_7$ cluster (14 $N\beta$). Upon decreasing and increasing the applied field, the magnetization curve exhibits a hysteresis loop with coercive field of ~541 Oe and remanent magnetization of 0.077 $N\beta$ (Figure S14 in the Supporting Information), which further confirms the occurrence of spontaneous magnetization of **2**·10$H_2O$. The canting angle is estimated to be about 0.315°, which is significantly larger than that of **1**·10$H_2O$.

However, for **3**·5$H_2O$ and **4**·5$H_2O$, the room temperature $\chi_M T$ values are 20.87 and 9.57 $cm^3$ K $mol^{-1}$ for **3**·5$H_2O$ and **4**·5$H_2O$, respectively, significantly higher than the spin-only values expected for seven isolated $Co^{II}$ ions and $Ni^{II}$ ions (Figures S7 and S8 in the Supporting Information). Unlike **1**·10$H_2O$ and **2**·10$H_2O$, the $\chi_M T$ values of **3**·5$H_2O$ and **4**·5$H_2O$ monotonously decrease upon temperature cooling, attaining 3.99 and 2.74 $cm^3$ K $mol^{-1}$ at 2 K, respectively, which indicates dominant antiferromagnetic interactions within and between the $Co^{II}_7$ or $Ni^{II}_7$ clusters. The magnetic susceptibilities of **3**·5$H_2O$ and **4**·5$H_2O$ do not show field-dependent behavior. Fitting the $\chi_M^{-1}$ versus $T$ data gives Curie constant $C$ = 25.12 $cm^3$ K $mol^{-1}$ and Weiss temperature $\theta$ = −59.84 K for **3**·5$H_2O$ and $C$ = 9.73 $cm^3$ K $mol^{-1}$ and $\theta$ = −3.42 K for **4**·5$H_2O$, respectively.

As we know, spin canting can arise from two mechanisms: the single-ion magnetic anisotropy and the antisymmetric exchange interaction.[21] Though $Co^{II}$ is an Ising-type ion with considerable anisotropy, this may not be the decisive factor that leads to spin canting because **1**·10$H_2O$ is canted antiferromagnetic but **3**·5$H_2O$ is not. In the present case, **1**·10$H_2O$ and **2**·10$H_2O$ crystallize in the polar space group *Pba*2 while **3**·5$H_2O$ and **4**·5$H_2O$ crystallize in the centrosymmetric space group *P*2/*n*, so the spin canted structures are only compatible with the crystal structures of **1**·10$H_2O$ and **2**·10$H_2O$, and the presence of inversion centers between the bridged $Co^{II}$ and $Ni^{II}$ ions in **3**·5$H_2O$ and **4**·5$H_2O$ forbids the occurrence of antisymmetric interactions. On the other hand, though a handful of $Ni^{II}$ complexes have been reported to display spin-canted behavior, the coexistence of spin canting and spin glass is particularly rare.[22]

**Sorption Properties.** To investigate the porosity of **1** and **2**, $N_2$ reversible adsorption measurements were carried out at 77 K on Micromeritics ASAP 2020 aparatus. The samples were first exchanged with dehydrated ethanol and then activated at 200 °C in vacuum, color changes from red to purple-blue and dark green to yellow-green were observed for **1** and **2**, respectively, indicating the loss of guest and coordinate water molecules and the formation of open $M^{II}$ sites (the frameworks remain intact as confirmed by PRXD, Figure S6 in the Supporting Information). Both activated samples show a typical type I adsorption isotherm,[23] indicating the presence of permanent microporosity (Figure 7 and Table 3). The $N_2$ adsorption data give a Langmuir surface area of 607 $m^2$ $g^{-1}$ and a BET surface area of 438 $m^2$ $g^{-1}$ for **1**, and a Langmuir surface area of 783 $m^2$ $g^{-1}$ and a BET surface area of 506 $m^2$ $g^{-1}$ for **2**, respectively. The maximal $N_2$ uptakes at 1 atm for **1** and **2** are 141.1 and 154.0 $cm^3$ $g^{-1}$, respectively, which suggest that the frameworks may have moderate affinities for $N_2$. This phenomenon encourages us to explore their potential capabilities on $H_2$ storage. At 77 K and 1 atm, remarkable $H_2$ uptakes of 114.8 (1.02 wt %) and 133.6 $cm^3$ $g^{-1}$ (1.20 wt %) for **1** and **2**, respectively, were determined, which are comparable

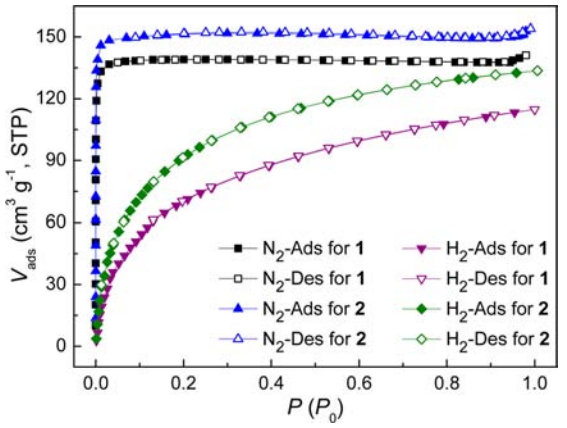


**Figure 7.** $N_2$ and $H_2$ adsorption isotherms for **1** and **2** at 77 K.

**Table 3. Adsorption and Isosteric Heat Data for 1 and 2**

| complex | BET[a] | $N_2$@77 K[b] | $H_2$@77 K[b] | $CO_2$@273 K[b] | $CO_2$@290 K[b] | $Q_{st}(CO_2)$[c] |
|---|---|---|---|---|---|---|
| **1** | 438 | 141.1 | 114.8 | 65.8 | 49.9 | 27.3 |
| **2** | 506 | 154.0 | 133.6 | 73.3 | 55.9 | 28.7 |

[a]Surface area, $m^2$ $g^{-1}$. [b]Adsorptive capability, $cm^3$ $g^{-1}$. [c]Isoteric heat of adsorption at 1 atm, kJ $mol^{-1}$.

to that of MOF-5 (1.32 wt %).[24] These uptakes roughly correlate to the established relation of 1 wt % $H_2$/500 $m^2$ $g^{-1}$ BET surface area.[25]

$CO_2$ adsorption on **1** and **2** was studied at 273 and 290 K, and was used to calculate the enthalpy of $CO_2$ adsorption. All $CO_2$ isotherms are also of type I. The uptake values of $CO_2$ for **1** and **2** are 65.8 $cm^3$ $g^{-1}$ (129.5 mg $g^{-1}$) and 73.3 $cm^3$ $g^{-1}$ (144.2 mg $g^{-1}$), respectively, at 273 K and 1 atm (Figure 8),

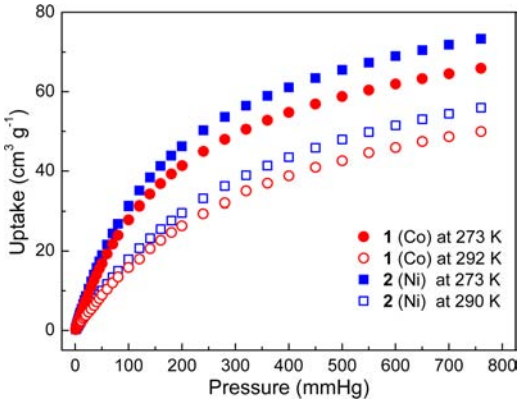


**Figure 8.** $CO_2$ adsorption isotherms for **1** and **2**.

which are larger than those of MOF-5 and many other microporous complexes.[26] At zero loading, the enthalpy of $CO_2$ adsorption is 27.3 kJ $mol^{-1}$ for **1** and 28.7 kJ $mol^{-1}$ for **2**, respectively, as estimated from the sorption isotherms at 273 and 290 K using the virial equation (Figures S14 and S15 in the Supporting Information), which are similar to those of HKUST-1 and MOFs with organic ammonium ions in the pores.[27] These values suggest high interaction energy between the quadrupolar $CO_2$ molecules and the possible open metal sites in **1** and **2**. It should be noticed that compound **2** shows relatively higher sorption capability than compound **1**, because


dx.doi.org/10.1021/ic401912k | *Inorg. Chem.* 2013, 52, 11573−11579

the open metal sites in activated compound **2** may show higher affinity for gas molecules than those in activated compound **1**.

## CONCLUSIONS

In summary, four eight-connected coordination polymers with heptanuclear structural units have been synthesized under hydrothermal conditions. **1**·10$H_2O$ exhibits spin-canted antiferromagnetism, and **2**·10$H_2O$ shows the coexistence of spin canting and spin-glass behavior, while **3**·5$H_2O$ and **4**·5$H_2O$ only display uniform antiferromagnetic properties. The occurrence of spin canting comes from the antisymmetric magnetic interactions. Besides, the activated samples of **1** and **2** show storage capacity for $H_2$ and $CO_2$. The results indicate a practical way to design and explore multifunctional materials featuring magnetic properties and gas storage.

## ASSOCIATED CONTENT

### Supporting Information

Crystal data in CIF format and figures. This material is available free of charge via the Internet at http://pubs.acs.org.

## AUTHOR INFORMATION

### Corresponding Author

*E-mail: taojun@xmu.edu.cn (J.T.).

### Notes

The authors declare no competing financial interest.

## ACKNOWLEDGMENTS

We are thankful for financial support from the NNSF of China (Grants 21021061 and 20923004) and the Specialized Research Fund for the Doctoral Program of Higher Education (Grant 20110121110012).

## REFERENCES

(1) (a) Murray, L. J.; Dinca, M.; Long, J. R. *Chem. Soc. Rev.* **2009**, *38*, 1294−1314. (b) Bux, H.; Liang, F. Y.; Li, Y. S.; Cravillon, J.; Wiebcke, M.; Caro, J. *J. Am. Chem. Soc.* **2009**, *131*, 16000−16001. (c) Deng, S.-G.; Saha, D.; Bao, Z.-B.; Jia, F. *Environ. Sci. Technol.* **2010**, *44*, 18201826. (d) Yaghi, O. M.; O'Keeffe, M.; Ockwig, N. W.; Chae, H. K.; Eddaoudi, M.; Kim, J. *Nature* **2003**, *423*, 705−714.

(2) (a) Lee, J.; Farha, O. K.; Roberts, J.; Scheidt, K. A.; Nguyen, S. T.; Hupp, J. T. *Chem. Soc. Rev.* **2009**, *38*, 1450−1459. (b) Fei, H.-H.; Rogow, D. L.; Oliver, S. R. J. *J. Am. Chem. Soc.* **2010**, *132*, 7202−7209. (c) Gándara, F.; Gomez-Lor, B.; Gutiérrez-Puebla, E.; Iglesias, M.; Monge, M. A.; Proserpio, D. M.; Snejko, N. *Chem. Mater.* **2008**, *20*, 72−78.

(3) (a) Halder, G. J.; Kepert, C. J.; Moubaraki, B.; Murray, K. S.; Cashion, J. D. *Science* **2002**, *298*, 1762−1765. (b) Zeng, M.-H.; Yao, M.-X.; Liang, H.; Zhang, W.-X.; Chen, X.-M. *Angew. Chem., Int. Ed.* **2007**, *46*, 1832−1835. (c) Li, J.; Tao, J.; Huang, R.-B.; Zheng, L.-S. *Inorg. Chem.* **2012**, *51*, 5988−5990.

(4) (a) Li, J.-R.; Tao, Y.; Yu, Q.; Bu, X.-H. *Chem. Commun.* **2007**, 1527−1529. (b) Hou, L.; Zhang, J.-P.; Chen, X.-M.; Ng, S.-W. *Chem. Commun.* **2008**, 4019−4021. (c) Fang, Q.-R.; Zhu, G.-S.; Jin, Z.; Xue, M.; Wei, X.; Wang, D.-J.; Qiu, S.-L. *Angew. Chem., Int. Ed.* **2006**, *45*, 6126−6130.

(5) Miller, J. S.; Drillon, M. *Magnetism: Molecules to Materials I−V*; Wiley-VCH: Weinheim, Germany, 2001.

(6) (a) Kampert, E.; Janssen, F. F. B. J.; Boukhvalov, D. W.; Russcher, J. C.; Smits, J. M. M.; de Gelder, R.; de Bruin, B.; Christianen, P. C. M.; Zeitler, U.; Katsnelson, M. I.; Maan, J. C.; Rowan, A. E. *Inorg. Chem.* **2009**, *48*, 11903−11908. (b) Beghidja, A.; Rogez, G.; Rabu, P.; Welter, R.; Drillon, M. *J. Mater. Chem.* **2006**, *16*, 2715−2728.

(7) (a) Eerenstein, W.; Mathur, N. D.; Scott, J. F. *Nature* **2006**, *442*, 759−765. (b) Singha, M. K.; Yanga, Y.; Takoudisa, C. G. *Coord. Chem. Rev.* **2009**, *253*, 2920−2934. (c) Rogez, G.; Viart, N.; Drillon, M. *Angew. Chem., Int. Ed.* **2010**, *49*, 1921−1923.

(8) Cui, H.-B.; Wang, Z.-M.; Takahashi, K.; Okano, Y.; Kobayashi, H.; Kobayashi, A. *J. Am. Chem. Soc.* **2006**, *128*, 15074−15075.

(9) Hou, L.; Zhang, W.-X.; Zhang, J.-P.; Xue, W.; Zhang, Y.-B.; Chen, X.-M. *Chem. Commun.* **2010**, *46*, 6311−6313.

(10) (a) Chen, Q.; Lin, J.-B.; Xue, W.; Zeng, M.-H.; Chen, X.-M. *Inorg. Chem.* **2011**, *50*, 2321−2328. (b) Ahnfeldt, T.; Guillou, N.; Gunzelmann, D.; Margiolaki, I.; Loiseau, T.; Férey, G.; Senker, J.; Stock, N. *Angew. Chem., Int. Ed.* **2009**, *48*, 5163−5166. (c) Gu, X.-J.; Lu, Z.-H.; Xu, Q. *Chem. Commun.* **2010**, *46*, 7400−7402. (d) Zhang, X.-M.; Fang, R.-Q.; Wu, H.-S. *J. Am. Chem. Soc.* **2005**, *127*, 7670−7671.

(11) Chen, Q.; Xue, W.; Wang, B.-Y.; Zeng, M.-H.; Chen, X.-M. *CrystEngComm* **2012**, *14*, 2009−2012.

(12) (a) Zhang, J.; Kang, Y.; Zhang, J.; Li, Z.-J.; Qin, Y.-Y.; Yao, Y.-G. *Eur. J. Inorg. Chem.* **2006**, 2253−2258. (b) Zhang, Y.-B.; Zhang, W.-X.; Feng, F.-Y.; Zhang, J.-P.; Chen, X.-M. *Angew. Chem., Int. Ed.* **2009**, *48*, 5287−5290. (c) Zhang, Y.-B.; Zhou, H.-L.; Lin, R.-B.; Zhang, C.; Lin, J.-B.; Zhang, J.-P.; Chen, X.-M. *Nat. Commun.* **2012**, *3*, 642−649.

(13) Sheldrick, G. M. *SHELXTL 6.12*; Bruker AXS, Inc.: Madison, WI, 2003.

(14) Spek, A. L. *PLATON, A Multipurpose Crystallographic Tool*; Utrecht University: Utrecht, The Netherlands, 2001.

(15) Blatov, V. A. *Struct. Chem.* **2012**, *23*, 955−963.

(16) Weng, D.-F.; Wang, Z.-M.; Gao, S. *Chem. Soc. Rev.* **2011**, *40*, 3157−3181.

(17) (a) Chen, X.-N.; Zhang, W.-X.; Chen, X.-M. *J. Am. Chem. Soc.* **2007**, *129*, 15738−15739. (b) Li, J.-R.; Yu, Q.; Tao, Y.; Bu, X.-H.; Ribas, J.; Batten, S. R. *Chem. Commun.* **2007**, 2290−2292.

(18) (a) Mondal, K. C.; Kostakis, G. E.; Lan, Y.; Anson, C. E.; Powell, A. K. *Inorg. Chem.* **2009**, *48*, 9205−9213. (b) Boonmak, J.; Nakano, M.; Chaichit, N.; Pakawatchai, C.; Youngme, S. *Inorg. Chem.* **2011**, *50*, 7324−7333.

(19) Bellitto, C.; Federici, F.; Colapietro, M.; Portalone, G.; Caschera, D. *Inorg. Chem.* **2002**, *41*, 709−714.

(20) Mydosh, J. A. *Spin Glasses: An Experimental Introduction*; Taylor and Francis: London, 1993.

(21) (a) Carlin, R. L. *Magnetochemistry*; Springer-Verlag: Berlin, Germany, 1986. (b) Lloret, F.; Munno, G.; De Julve, M.; Cano, J.; Ruiz, R.; Caneschi, A. *Angew. Chem., Int. Ed.* **1998**, *37*, 135−138. (c) Jia, L.-H.; Liu, A.-C.; Wang, B.-W.; Wang, Z.-M.; Gao, S. *Polyhedron* **2011**, *30*, 3112−3115.

(22) (a) Liu, X.-T.; Wang, X.-Y.; Zhang, W.-X.; Cui, P.; Gao, S. *Adv. Mater.* **2006**, *18*, 2852−2856. (b) Huang, F.-P.; Tian, J.-L.; Li, D.-D.; Chen, G.-J.; Gu, W.; Yan, S.-P.; Liu, X.; Liao, D.-Z.; Cheng, P. *Inorg. Chem.* **2010**, *49*, 2525−2529.

(23) Sing, K. S. W.; Everett, D. H.; Haul, R. A. W.; Mouscou, L.; Rouquerol, J.; Siemieniewska, I. *Pure Appl. Chem.* **1985**, *57*, 603−619.

(24) Rowsell, J. L. C.; Millward, A. R.; Park, K. S.; Yaghi, O. M. *J. Am. Chem. Soc.* **2004**, *126*, 5666−5667.

(25) Hirscher, M. *Handbook of Hydrogen Storage*; Wiley-VCH: Weinheim, 2010.

(26) (a) Demessence, A.; D'Alessandro, D. M.; Foo, M. L.; Long, J. R. *J. Am. Chem. Soc.* **2009**, *131*, 8784−8786. (b) Tan, Y.-X.; He, Y.-P.; Zhang, J. *Inorg. Chem.* **2011**, *50*, 11527−11531.

(27) (a) Moellmer, J.; Moeller, A.; Dreisbach, F.; Gläser, R.; Staudt, R. *Microporous Mesoporous Mater.* **2011**, *138*, 140. (b) An, J.; Rosi, N. L. *J. Am. Chem. Soc.* **2010**, *132*, 5578−5579.